Letter

Precision characterization of the $^2D_{5/2}$ state and the quadratic Zeeman coefficient in $^{171}Yb^+$

T. R. Tan,[1,*] C. L. Edmunds,[2,†] A. R. Milne,[2,‡] M. J. Biercuk,[2] and C. Hempel[2,3,§]

[1]*The University of Sydney, School of Physics, NSW, 2006, Australia*

[2]*ARC Centre of Excellence for Engineered Quantum Systems, The University of Sydney, School of Physics, NSW, 2006, Australia*

[3]*The University of Sydney Nano Institute (Sydney Nano), The University of Sydney, NSW 2006, Australia*

(Received 28 December 2020; accepted 14 July 2021; published 30 July 2021)

We report measurements of the branching fraction, hyperfine constant, and second-order Zeeman coefficient of the $D_{5/2}$ level in $^{171}Yb^+$ with up to a two-orders-of-magnitude reduction in uncertainty compared to previously reported values. We estimate the electric quadrupole reduced matrix element of the $S_{1/2} \leftrightarrow D_{5/2}$ transition to be 12.5(4) ea_0^2. Furthermore, we determine the transition frequency of the $F_{7/2} \leftrightarrow {}^1D[3/2]_{3/2}$ at 760 nm with a ∼25-fold improvement in uncertainty. These measurements provide benchmarks for quantum-many-body atomic-physics calculations and provide valuable data for efforts to improve quantum information processors based on $^{171}Yb^+$.

DOI: 10.1103/PhysRevA.104.L010802

I. INTRODUCTION

Trapped atomic ions combine the benefits of long storage time and excellent isolation from the environment, providing an attractive physical system for numerous applications in quantum technology [1,2]. Among the singly charged ions most commonly investigated, $^{171}Yb^+$has found applications in tests of fundamental physics [3,4], frequency metrology [5,6], and quantum information processing (QIP) [7–10]. All of these applications rely on a deep understanding of atomic structure theory, which is guided by and refined through precision measurements [11–18]. However, accurate calculation of the atomic properties for $^{171}Yb^+$has proven to be highly challenging due to its large number of valence electrons and complications arising from mixing between electronic configurations [15], making it a particularly interesting system for experimental investigation.

The nuclear spin of $^{171}Yb^+$is one-half, causing the $^2S_{1/2}$ electronic ground state to split into a hyperfine doublet separated by ∼12.64 GHz. Its metastable levels (Fig. 1) include $^2D_{3/2}$, $^2D_{5/2}$, and $^2F_{7/2}$ with lifetimes of 52.7 ms [19], 7.2 ms [20], and $\gtrsim$ 5.4 years [21], respectively. The short lifetime of $^2D_{5/2}$ has made the state less attractive for frequency metrology compared to $^2D_{3/2}$ [22–24] and $^2F_{7/2}$ [5,25,26]; experimental measurements on $^2D_{5/2}$ were last reported more than 20 years ago [27]. Still, measurements with improved precision provide a good benchmark to verify challenging and model-dependent atomic-physics calculations. Furthermore, the metastable ^2D levels in $^{171}Yb^+$provide extra degrees of freedom for applications in QIP. These find use in implementing entangling gate operations [28] or to scalably improve qubit measurement fidelities with minimal technical overhead [29].

In this article we report precision measurements on branching ratios, the electric quadrupole (E2) reduced matrix element, the quadratic Zeeman (QZ) coefficient, and the hyperfine splitting of the $^2D_{5/2}$ state in $^{171}Yb^+$, with up to two orders of magnitude reduction in uncertainty compared to the previously best reported values. Our spectroscopic experiments use a single ion in a Paul trap with a storage lifetime of several months and a stabilized solid-state laser near 411 nm. Furthermore, we provide a more precise measurement of the transition between $^2F_{7/2} \leftrightarrow {}^1D[3/2]_{3/2}$ at 760 nm than previously reported [30–32].

II. EXPERIMENTAL SETUP

The experimental setup is detailed in Ref. [33]. A permanent magnet produces a quantization field of ∼0.44 mT at the ion position, which we infer using the 13.98(1)-GHz/T linear Zeeman shift of the $^2S_{1/2}$ stretched states [34,35]. A 369.5-nm laser in conjunction with electro-optic modulators (EOMs) is used for Doppler cooling, state preparation, and detection. Separate 369.5-nm laser beamlines allow for selective measurements of just the population in $^2S_{1/2}|F = 1\rangle$ using the "standard detection" (SD) or the entire $^2S_{1/2}$ "manifold detection" (MD). A 935-nm laser continuously repumps the population which has decayed into the $^2D_{3/2}$ manifold.

We drive the $^2S_{1/2} \leftrightarrow {}^2D_{5/2}$ transition using an external-cavity diode laser at 411 nm, which is locked to an ultralow expansion reference cavity with a free spectral range (FSR) of 1.5 GHz, a finesse of approximately 32,000, and a frequency drift rate of ∼ 320 mHz/s. An additional, cavity-stabilized 760-nm diode laser configured with a cat-eye reflector [36,37] is used to provide efficient repumping from the long-lived $^2F_{7/2}$ via $^1D[3/2]_{3/2}$, which has a lifetime of ∼ 28.6 ns and decays primarily to the $^2S_{1/2}$ ground states [30,38]. To maximize repumping efficiency, an EOM driven at 5.258 GHz is used to create an additional laser frequency component, matching

*tingrei86@gmail.com

†Present address: Institute for Experimental Physics, University of Innsbruck, Innsbruck 6020, Austria; edmunds.claire@gmail.com

‡Present address: Q-CTRL Pty Ltd, Sydney, New South Wales 2006, Australia.

§Present address: Paul Scherrer Institut, Villigen PSI CH-5232, Switzerland; cornelius.hempel@gmail.com

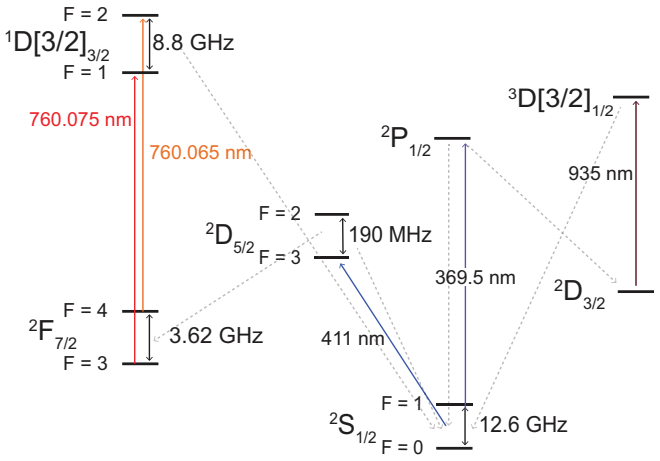

FIG. 1. Selected energy levels and transition wavelengths in ^{171}Yb$^+$. Dashed lines show relevant decay channels. Our work focuses on the 411-nm electric quadrupole (E2) $^2S_{1/2} \leftrightarrow {}^2D_{5/2}$ transition. The $^2D_{5/2}|F=3\rangle$ decays to $^2S_{1/2}|F=1\rangle$ and $^2F_{7/2}|F=3,4\rangle$, and $^2D_{5/2}|F=2\rangle$ decays to $^2S_{1/2}|F=0,1\rangle$ and $^2F_{7/2}|F=3\rangle$. A 760-nm laser is used for fast repumping of $^2F_{7/2}$ to $^2S_{1/2}$ via $^1D[3/2]_{3/2}$. Some hyperfine structures and Zeeman sublevels are omitted for clarity.

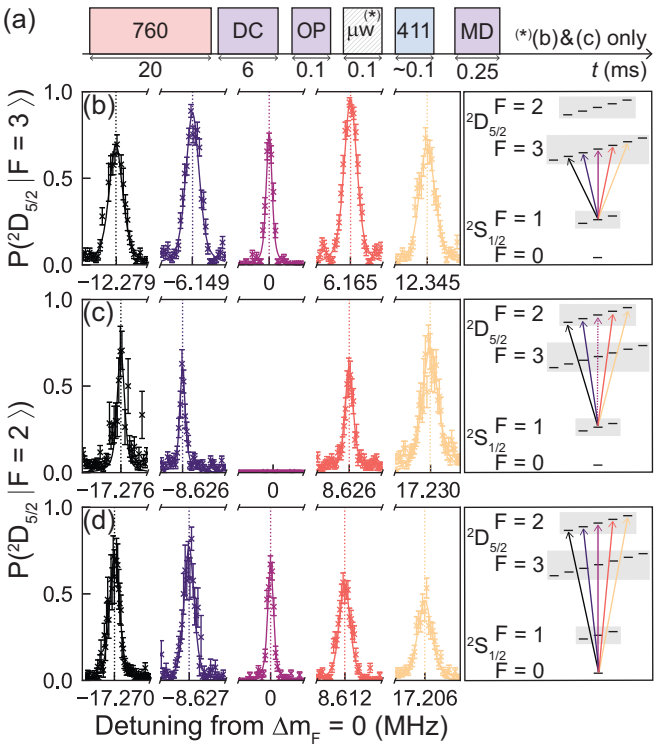

FIG. 2. Spectra of the $^2S_{1/2} \leftrightarrow {}^2D_{5/2}$ transitions at 411 nm. (a) The spectroscopy pulse sequence including 760-nm repumping, Doppler cooling (DC), optical pumping to prepare $^2S_{1/2}|F=0\rangle$ (OP), microwave excitation to $^2S_{1/2}|F=1, m_F=0\rangle$ in select cases (μw), the 411-nm spectroscopy pulse and detection (MD), which includes the same frequency components as DC but is tuned closer to resonance. (b,c,d) 411-nm laser frequency scans around the line center at $\Delta m_F = 0$ for the different hyperfine transitions indicated in corresponding colors on the right. In (c), the $\Delta m_F = 0$ transition cannot be driven due to atomic selection rules. Error bars are calculated from quantum projection noise (QPN), and the data are fitted to Voigt profiles. The full width at half maximum of the lines varies between 3 and 11 kHz, with the largest impact arising from laser-polarization-dependent coupling strength differences across different transitions. The uncertainties of the indicated center frequencies are limited by the fitting error to (0.1–2) kHz; amplitude differences are due to polarization and beam orientation with respect to the quantization axis.

the hyperfine splittings of 3.620 GHz [39,40] and 8.8 GHz [32] for $^2F_{7/2}$ and $^1D[3/2]_{3/2}$, respectively. The 5.258-GHz microwave signal used to drive the EOM is tuned by maximizing fluorescence counts on the 369.5-nm detection transition while simultaneously illuminating the ion with 411- and 760-nm light. With an intensity of ~ 0.63 W/mm^2, the typical repumping time from the $^2F_{7/2}$ state to the $^2S_{1/2}$ manifold is ~20 ms, significantly faster than other repumping channels [19,20,30,41], such as the 638-nm transition to $^1D[5/2]_{5/2}$. All laser beams are controlled by acousto-optic modulators driven by direct digital synthesis sources referenced to a rubidium frequency standard.

III. SPECTROSCOPY OF THE $^2S_{1/2} \leftrightarrow {}^2D_{5/2}$ TRANSITION

We begin by performing spectroscopy on the $^2S_{1/2} \leftrightarrow {}^2D_{5/2}$ optical transition near 411 nm, resolving individual hyperfine and Zeeman levels as shown in Fig. 2. The ion is initialized in $^2S_{1/2}|F=0\rangle$ by optical pumping and optionally transferred to $^2S_{1/2}|F=1, m_F=0\rangle$ through application of a microwave π pulse. The typical 411-nm π-pulse duration ranges from about 17 to 25 μs, depending on the available coupling strength to the transition in question, which is set by polarization and beam direction with respect to the quantization magnetic field. After applying a 411-nm spectroscopy pulse of fixed duration, state-dependent fluorescence is induced by a 369.5-nm (MD) pulse that distinguishes population in the $^2S_{1/2}$ manifold ("bright") from that in other levels ("dark"). A 20-ms pulse at 760 nm is applied to repump population decayed to $^2F_{7/2}$ at the beginning of each measurement cycle. The center frequency for each transition is extracted by fitting the spectroscopic peaks to Voigt profiles. We measure a frequency of 729.487 752(178) THz for the $^2S_{1/2}|F=0\rangle \leftrightarrow {}^2D_{5/2}|F=2, m_F=0\rangle$ transition, which we report with ± 0.1 pm uncertainty as per our wavemeter's maximum guaranteed accuracy when the measurement wavelength is more than $\pm$ 200 nm away from the calibration wavelength at 632 nm. Using the previously published transition frequency with ~150 kHz uncertainty [27] as a reference, we find our wavemeter's accuracy to be within ~30 MHz. We note that an accurate measurement of the $^2S_{1/2} \leftrightarrow {}^2D_{5/2}$ transition in the ^{172}Yb$^+$ isotope has recently been reported with an uncertainty of 4 Hz [42].

IV. LIFETIME AND BRANCHING RATIO OF $^2D_{5/2}$

The lifetimes and decay branching ratios of $^2D_{5/2}$ are measured by a sequence that initializes in $^2D_{5/2}|F=2\rangle$ or $^2D_{5/2}|F=3\rangle$ through multiple sequential π pulses to different Zeeman sublevels, followed by an immediate detection used for postselection on events with successful transfer, see

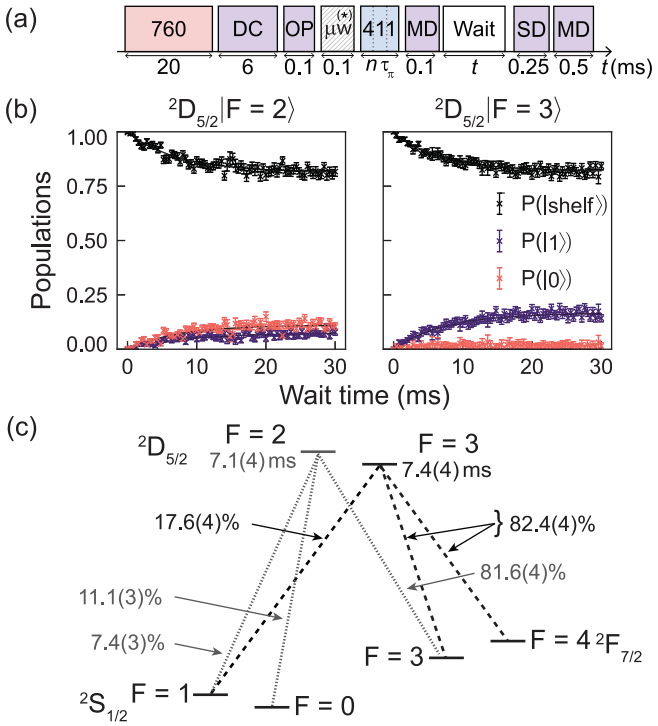

FIG. 3. Lifetime and branching ratio measurements. (a) Measurement pulse sequence similar to Fig. 2(a), with an added variable wait time t, bracketed by "manifold detection" (MD) and "state detection" (SD) pulses for postselection and measurement of branching to the two $^2S_{1/2}$ levels, respectively. A series of $n = 5$ π-pulses on the accessible 411-nm transitions to different Zeeman sublevels maximizes the shelving success to $^2D_{5/2}\,|F = 2\rangle$. Due to the similar Zeeman splitting in $^2S_{1/2}\ |F = 1\rangle$ and $^2D_{5/2}\ |F = 3\rangle$ manifolds, a similar $n = 3$ procedure is used to prepare $^2D_{5/2}\,|F = 3\rangle$ from $^2S_{1/2}\,|F = 1, m_F = 0\rangle$. (b) State decay curves as a function of wait time after initialization of the target state. The populations P($|0\rangle$) and P($|1\rangle$) refer to the two hyperfine levels in the $^2S_{1/2}$ ground-state manifold, while P($|$shelf$\rangle$) refers to the shelved population in $^2D_{5/2}$ or $^2F_{7/2}$. (c) Overview of the decay channels and branching fractions measured in this work.

Fig. 3(a). Following a variable wait time, two final detection pulses determine the population in the $^2S_{1/2}$ states and shelved manifolds. The lifetime is extracted by fitting exponential decays, weighted by QPN, to time-delayed data [Figs. 3(b) and 3(c)], where we take the asymptotic limits of the fit as branching ratios. The values agree with previous measurements on different isotopes, which we summarize in Table I. The asymptotic limits for the $|F = 0\rangle$ and $|F = 1\rangle$ populations are 11.1(3)% and 7.4(3)%, which agree well with the expected relative decay branching fraction from $^2D_{5/2}\,|F = 2, m_F = 0\rangle$ to $^2S_{1/2}\,|F = 1\rangle$ and $^2D_{5/2}\,|F = 2, m_F = 0\rangle$ to $^2S_{1/2}\,|F = 0\rangle$. From the lifetime and branching ratios, we estimate the E2 reduced matrix element to be 12.5(4) ea_0^2, with e and a_0 the elementary charge and Bohr radius, respectively, which is consistent with theoretical predictions [13,43].

V. HYPERFINE SPLITTING OF $^2D_{5/2}$

The hyperfine splitting of $^2D_{5/2}$ can be deduced from the difference of the transition frequencies between

TABLE I. Branching ratios and lifetimes for the $^2D_{5/2}\,|F = 2, 3\rangle$ state contrasted with previous measurements and a theoretical prediction. Uncertainties of 1σ are derived from exponential fits to the state evolution shown in Fig. 3.

	Decay to $^2S_{1/2}$	Decay to $^2F_{7/2}$	Lifetime (ms)
This work (exp.) $^{171}Yb^+\,|F = 3\rangle$	17.6(4)%	82.4(4)%	7.1(4)
This work (exp.) $^{171}Yb^+\,|F = 2\rangle$	18.4(4)%	81.6(4)%	7.4(4)
Taylor *et al.* [20] (1997 exp.) $^{172}Yb^+$	17(4)%	83(3)%	7.2(3)
Yu and Maleki [19] (2000 exp.) $^{174}Yb^+$	–	–	7.0(4)
Fawcett and Wilson [11] (1991 calc.) Yb II	19.7%	80.3%	5.74

$^2S_{1/2}\,|F = 1, m_F = 0\rangle$ and $^2D_{5/2}\,|F = 2, m_F = 0\rangle$ as well as $^2D_{5/2}\,|F = 3, m_F = 0\rangle$. Electric quadrupole transition selection rules forbid the $^2S_{1/2}\,|F = 1, m_F = 0\rangle \leftrightarrow {}^2D_{5/2}\,|F = 2, m_F = 0\rangle$ transition to be directly driven; therefore we infer its value from measurements of $^2S_{1/2}\,|F = 1, m_F = 0\rangle \leftrightarrow {}^2D_{5/2}\,|F = 2, m_F = \pm 1\rangle$. The frequency of the 411-nm laser is stabilized to the same cavity mode throughout this measurement in order to avoid uncertainties from wavemeter's accuracy or cavity's FSR in the determination of hyperfine splitting. All transition frequencies are corrected for cavity drift over the measurement duration of ∼4 h and QZ shifts at the B field of 441.26(2) μT [44]. From our measurements we extract a hyperfine splitting of $\Delta_{\mathrm{HF},D} = -190.104(3)$ MHz and, correspondingly, a hyperfine constant of $A_{D,5/2} = -63.368(1)$ MHz. This measurement is more than two orders of magnitude more precise than the best previously reported value of −191(2) MHz [27] and limited by the uncertainties of the QZ coefficients and fitting errors. Table II summarizes both measured and theoretical values for $A_{D,5/2}$, illustrating the difficulty of performing exact calculations for $^{171}Yb^+$.

VI. QUADRATIC ZEEMAN COEFFICIENT

To deduce the second-order Zeeman coefficient of the $^2D_{5/2}\,|F = 3, m_F = 0\rangle$ state, we vary the magnetic field at the ion location over an interval of ∼ [0.44,1] mT through

TABLE II. Comparison of measurements and calculations of the $^2D_{5/2}$ hyperfine constant.

Reference		$A_{D,5/2}$ (MHz)
This work	(2020 experiment)	–63.368(1)
Roberts *et al.* [27]	(1999 experiment)	–63.6(7)
Nandy and Sahoo [17]	(2014 calculation)	–69(6)
Porsev *et al.* [15]	(2012 calculation)	–96
Sahoo and Das [13]	(2011 calculation)	–48(15)
Itano [12]	(2006 calculation)	–12.58

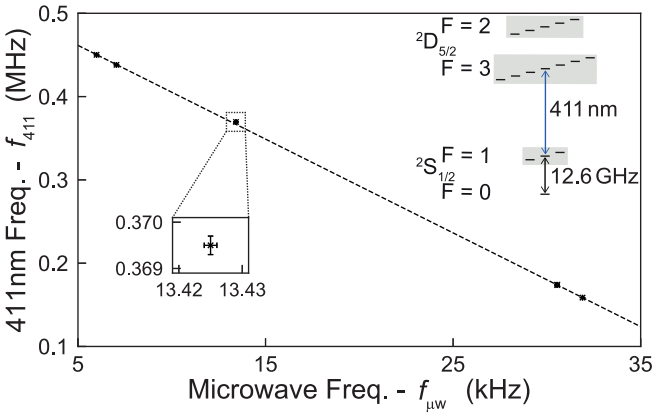

FIG. 4. Frequency of $^2D_{5/2}|F=3,m_F=0\rangle$ near 411-nm vs frequency of $^2S_{1/2}|F=1,m_F=0\rangle$ with respect to $^2S_{1/2}|F=0\rangle$ at different magnetic field strengths. They are deduced from the $^2S_{1/2}|F=1,m_F=1\rangle \leftrightarrow {}^2D_{5/2}|F=3,m_F=0\rangle$ and the $^2S_{1/2}|F=0\rangle \leftrightarrow {}^2S_{1/2}|F=1,m_F=0\rangle$ transitions, which are illustrated on the right. Typical statistical uncertainties of the frequency measurements are approximately 200 Hz and 0.2 Hz for the optical and microwave frequencies, respectively, with the error-bar size highlighted in the lower inset. The frequency offsets used for plotting are $f_{\mu w}=12.642\,812\,118\,466$ GHz, and $f_{411}=729.487\,559$ THz. We deduce a slope of –11.27(4) where the uncertainty is the standard error of the fit.

adjustment of a permanent magnet's placement. For each B-field configuration, the frequencies of the $^2S_{1/2}|F=0\rangle \leftrightarrow {}^2S_{1/2}|F=1,m_F=0\rangle$ hyperfine transition at ~12.6 GHz and the $^2S_{1/2}|F=1,m_F=0\rangle \leftrightarrow {}^2D_{5/2}|F=3,m_F=0\rangle$ transition at 411 nm are recorded, updated, and averaged through interleaved Ramsey interrogations using wait times of 50 and 0.1 ms, respectively. Similar to the hyperfine splitting measurement, the 411-nm laser frequency is stabilized to the same cavity mode throughout this measurement over different B fields. We combine the microwave and optical frequency measurements to determine the energy difference between the $^2D_{5/2}|F=3,m_F=0\rangle$ and $^2S_{1/2}|F=0\rangle$ states. In Fig. 4 we plot the relative frequency shifts of $^2S_{1/2}|F=0\rangle \leftrightarrow {}^2D_{5/2}|F=3,m_F=0\rangle$ and $^2S_{1/2}|F=0\rangle \leftrightarrow {}^2S_{1/2}|F=1,m_F=0\rangle$ after compensating the measured optical frequencies for cavity drift. We determine the ratio of the quadratic Zeeman coefficients to be –11.27(4). Taken together with the often quoted value of 0.031 08 Hz/μT^2 [45] for the quadratic Zeeman coefficient in the $^2S_{1/2}$ ground-state transition, this yields a QZ coefficient of $-0.350(1)$ Hz/μT^2 for $^2D_{5/2}|F=3,m_F=0\rangle$ with respect to the $^2S_{1/2}|F=0\rangle$ ground state. The quadratic Zeeman coefficient of $^2D_{5/2}|F=3,m_F=0\rangle$ is

$$\frac{1}{4}\frac{(g_{J,D}-g_I)^2\mu_B^2}{h^2\Delta_{\mathrm{HF},D}}, \tag{1}$$

which has the same magnitude but opposite sign as $^2D_{5/2}|F=2,m_F=0\rangle$ [44]; here, $\Delta_{\mathrm{HF},D}$, $g_{J,D}$, and μ_B are the hyperfine splitting, Landé g factor of $^2D_{5/2}$, and Bohr's magneton, respectively. The nuclear g factor of Yb^+ is $g_I=-5.38\times10^{-4}$ [46]. The absolute value of our measurement is an order of magnitude more accurate than the best published result of 0.38(8) Hz/μT^2 measured on $^2S_{1/2}|F=0\rangle \leftrightarrow {}^2D_{5/2}|F=2,m_F=0\rangle$ [27]. We further quantified a potential AC Zeeman shift in the transition frequencies due to the trap's radio-frequency field using an Autler-Townes spectroscopy method first demonstrated in Ref. [47]. The magnitude of the B field perpendicular to the quantization axis oscillating at the trapping radio frequency is measured to be less than 10 nT, having a negligible impact on our measurements.

The quadratic Zeeman coefficient of the ground-state transition is

$$QZ_S=\frac{1}{2}\frac{(g_{J,S}-g_I)^2\mu_B^2}{h^2\Delta_{\mathrm{HF},S}}, \tag{2}$$

where $\Delta_{\mathrm{HF},S}=12.642\,812\,118\,466$ GHz [6] is the hyperfine splitting of the $^2S_{1/2}$ ground state and $g_{J,S}$ is the Landé g factor for $^2S_{1/2}$. The quadratic Zeeman coefficient of $^2D_{5/2}|F=3,m_F=0\rangle$ with respect to the $^2S_{1/2}|F=0\rangle$ ground state is

$$QZ_{D,F=3}=\frac{1}{4}\frac{(g_{J,D}-g_I)^2\mu_B^2}{h^2\Delta_{\mathrm{HF},D}}-\left(-\frac{1}{4}\frac{(g_{J,S}-g_I)^2\mu_B^2}{h^2\Delta_{\mathrm{HF},S}}\right). \tag{3}$$

A recent theory calculation of g-factor anomalies in $^{171}Yb^+$ gives $g_{J,S}=2.0031(3)$ and $g_{J,D}=1.200\,51(2)$, where the uncertainties are the estimated maximum error of the calculation [16]. Using these values we evaluate the QZ coefficients to $QZ_S=0.031\,10(1)$ Hz/μT^2 and $QZ_{D,F=3}=-0.356\,06(1)$ Hz/μT^2, yielding a ratio of the quadratic Zeeman coefficient of –11.448(2), which does not agree with our measurement in Fig. 4. This could indicate an effect not captured by Eqs. (2) and (3), or a discrepancy in the g_J values above. Spectroscopic measurement values of $g_{J,S}$ and $g_{J,D}$ were given by Meggers as 1.998 and 1.202 [35] without specifying uncertainties. Assuming an uncertainty of 0.002 for both values, we evaluate the QZ coefficients and ratio to be $QZ_S=0.030\,94(4)$ Hz/μT^2, $QZ_{D,F=3}=$ –0.3571(12) Hz/μT^2, and –11.54(4), which also does not agree with our observations. Our measurements notwithstanding, we note that Meggers' ground-state g-factor value of 1.998 implies a g-factor anomaly correction of -4×10^{-3}, which is of opposite sign to the $\delta g=+79.8\times10^{-5}$ reported in Ref. [16]. This suggests potential issues in previous g-factor measurements in Yb^+.

VII. SPECTROSCOPY OF THE $^2F_{7/2} \leftrightarrow {}^1D[3/2]_{3/2}$ TRANSITION

As a final measurement, we determine the $^2F_{7/2} \leftrightarrow {}^1D[3/2]_{3/2}$ transition near 760 nm, used to repump population to $^2S_{1/2}$. We first prepare population in $^2D_{5/2}|F=2,m_F=0\rangle$ using a 411-nm laser pulse, followed by a 10-ms wait time to allow for decay to $^2F_{7/2}|F=3\rangle$. A subsequent brief application of the 369.5-nm MD beam allows us to exclude instances of decay to $^2S_{1/2}$ from the data in postprocessing. A 760-nm laser pulse is then applied to induce a transition to the short-lived $^1D[3/2]_{3/2}$ level, which primarily decays to $^2S_{1/2}$. Successful repump events then yield fluorescence under application of the 369.5-nm MD light. We repeat this procedure with a state preparation in $^2D_{5/2}|F=3,m_F=0\rangle$, where the population decays to both $^2F_{7/2}|F=3\rangle$ and $^2F_{7/2}|F=4\rangle$.

The measured center frequencies are

$$^2F_{7/2}\,|F=3\rangle \leftrightarrow {}^1D[3/2]_{3/2}\,|F=1\rangle : 394.424\,943(20)\text{THz},$$

$$^2F_{7/2}\,|F=4\rangle \leftrightarrow {}^1D[3/2]_{3/2}\,|F=2\rangle : 394.430\,203(16)\text{THz},$$

respectively. Here the uncertainties are dominated by line broadening due to our inability to prepare the ion in a specific $^2F_{7/2}$ Zeeman level as well as the wavemeter's specified absolute accuracy, which is 10 MHz within ± 200 nm of the calibration wavelength of 632 nm. These measurements provide a 25-fold reduction in uncertainty over previously reported values [32].

VIII. CONCLUSION

In conclusion, we report measurements of the hyperfine splitting, branching ratios, and quadratic Zeeman coefficient of $^2D_{5/2}$ in $^{171}Yb^+$with improved precision and investigate the 760-nm transition to efficiently depopulate the $^2F_{7/2}$ state. These results can be used to benchmark and verify quantum-many-body calculations in Yb^+, e.g., in support of studies of parity nonconserving physics and the related nuclear anapole moment [13–16,18]. Furthermore, these results provide the necessary characterizations required for improving the measurement fidelity of $^{171}Yb^+$hyperfine qubits, as detailed in our separate manuscript Ref. [29].

ACKNOWLEDGMENTS

T.R.T. acknowledges support from the Sydney Quantum Academy. The authors thank A. Singh and T. F. Wohlers-Reichel for their contribution to assembling and maintenance of the experimental setup. This work was partially supported by the Intelligence Advanced Research Projects Activity Grant No.W911NF-16-1-0070, the U.S. Army Research Office Grant No. W911NF-14-1-0682, the Australian Research Council Centre of Excellence for Engineered Quantum Systems Grant No. CE170100009, and a private grant from H. & A. Harley.

T.R.T. and C.E. contributed equally to this work.

[1] D. J. Wineland, C. Monroe, W. M. Itano, D. Leibfried, B. E. King, and D. M. Meekhof, Experimental issues in coherent quantum-state manipulation of trapped atomic ions, J. Res. Nat. Inst. Stand. Technol. **103**, 259 (1998).

[2] M. Knoop, L. Hilico, and J. Eschner, Modern applications of trapped ions, J. Phys. B: At. Mol. Opt. Phys. **42**, 150201 (2009).

[3] V. V. Flambaum, A. J. Geddes, and A. V. Viatkina, Isotope shift, nonlinearity of King plots, and the search for new particles, Phys. Rev. A **97**, 032510 (2018).

[4] I. Counts, J. Hur, D. P. L. Aude Craik, H. Jeon, C. Leung, J. C. Berengut, A. Geddes, A. Kawasaki, W. Jhe, and V. Vuletić, Evidence for Nonlinear Isotope Shift in Yb^+ Search for New Boson, Phys. Rev. Lett. **125**, 123002 (2020).

[5] N. Huntemann, C. Sanner, B. Lipphardt, Chr. Tamm, and E. Peik, Single-Ion Atomic Clock with 3×10^{-18} Systematic Uncertainty, Phys. Rev. Lett. **116**, 063001 (2016).

[6] P. T. H. Fisk, M. J. Sellars, M. A Lawn, and G. Coles, Accurate measurement of the 12.6 GHz "clock" transition in trapped $^{171}Yb^+$ ions, IEEE Trans. Ultrason. Ferroelectr. Freq. Control **44**, 344 (1997).

[7] A. Soare, H. Ball, H. D. Hayes, D. J. Sastrawan, M. C. Jarratt, J. J. McLoughlin, X. Zhen, T. J. Green, and M. J. Biercuk, Experimental noise filtering by quantum control, Nat. Phys. **10**, 825 (2014).

[8] S. Olmschenk, K. C. Younge, D. L. Moehring, D. Matsukevich, P. Maunz, and C. Monroe, Manipulation and detection of a trapped Yb^+ hyperfine qubit, Phys. Rev. A **76**, 052314 (2007).

[9] S. Mavadia, C. L. Edmunds, C. Hempel, H. Ball, F. Roy, T. M. Stace, and M. J. Biercuk, Experimental quantum verification in the presence of temporally correlated noise, NPJ Quantum Inf. **4**, 7 (2018).

[10] C. Monroe, W. C. Campbell, L.-M. Duan, Z.-X. Gong, A. V. Gorshkov, P. W. Hess, R. Islam, K. Kim, N. M. Linke, G. Pagano, P. Richerme, C. Senko, and N. Y. Yao, Programmable quantum simulations of spin systems with trapped ions, Rev. Mod. Phys. **93**, 025001 (2021).

[11] B. C. Fawcett and M. Wilson, Computed oscillator strengths, Landé g values, and lifetimes in Yb II, At. Data Nucl. Data Tables **47**, 241 (1991).

[12] Wayne M. Itano, Quadrupole moments and hyperfine constants of metastable states of Ca^+, Sr^+, Ba^+, Yb^+, Hg^+, and Au, Phys. Rev. A **73**, 022510 (2006).

[13] B. K. Sahoo and B. P. Das, Parity nonconservation in ytterbium ion, Phys. Rev. A **84**, 010502(R) (2011).

[14] V. A. Dzuba and V. V. Flambaum, Calculation of nuclear-spin-dependent parity nonconservation in *s–d* transitions of Ba^+, Yb^+, Ra^+, Phys. Rev. A **83**, 052513 (2011).

[15] S. G. Porsev, M. S. Safronova, and M. G. Kozlov, Correlation effects in Yb^+ and implications for parity violation, Phys. Rev. A **86**, 022504 (2012).

[16] G. H. Gossel, V. A. Dzuba, and V. V. Flambaum, Calculation of strongly forbidden M1 transitions and g-factor anomalies in atoms considered for parity-nonconservation measurements, Phys. Rev. A **88**, 034501 (2013).

[17] D. K. Nandy and B. K. Sahoo, Quadrupole shifts for the $^{171}Yb^+$ ion clocks: Experiments versus theories, Phys. Rev. A **90**, 050503(R) (2014).

[18] B. M. Roberts, V. A. Dzuba, and V. V. Flambaum, Nuclear-spin-dependent parity nonconservation in s-$d_{5/2}$ and s-$d_{3/2}$ transitions, Phys. Rev. A **89**, 012502 (2014).

[19] N. Yu and L. Maleki, Lifetime measurements of the $4f^{14}5d$ metastable states in single ytterbium ions, Phys. Rev. A **61**, 022507 (2000).

[20] P. Taylor, M. Roberts, S. V. Gateva-Kostova, R. B. M. Clarke, G. P. Barwood, W. R. C. Rowley, and P. Gill, Investigation of the $^2S_{1/2}$–$^2D_{5/2}$ clock transition in a single ytterbium ion, Phys. Rev. A **56**, 2699 (1997).

[21] M. Roberts, P. Taylor, G. P. Barwood, W. R. C. Rowley, and P. Gill, Observation of the $^2S_{1/2}$–$^2F_{7/2}$ electric octupole transition in a single $^{171}Yb^+$ ion, Phys. Rev. A **62**, 020501(R) (2000).

[22] S. Webster, R. Godun, S. King, G. Huang, B. Walton, V. Tsatourian, H. Margolis, S. Lea, and P. Gill, Frequency

measurement of the $^2S^2_{1/2}D_{3/2}$ electric quadrupole transition in a single $^{171}Yb^+$ ion, IEEE Trans. Ultras. Ferroelectr. Freq. Control **57**, 592 (2010).

[23] Chr. Tamm, N. Huntemann, B. Lipphardt, V. Gerginov, N. Nemitz, M. Kazda, S. Weyers, and E. Peik, Cs-based optical frequency measurement using cross-linked optical and microwave oscillators, Phys. Rev. A **89**, 023820 (2014).

[24] M. Schacht, J. R. Danielson, S. Rahaman, J. R. Torgerson, J. Zhang, and M. M. Schauer, $^{171}Yb^+$ $5D_{3/2}$ hyperfine state detection and $F = 2$ lifetime, J. Phys. B **48**, 065003 (2015).

[25] K. Hosaka, S. A. Webster, A. Stannard, B. R. Walton, H. S. Margolis, and P. Gill, Frequency measurement of the $^2S_{1/2}$−$^2F_{7/2}$ electric octupole transition in a single $^{171}Yb^+$ ion, Phys. Rev. A **79**, 033403 (2009).

[26] N. Huntemann, M. Okhapkin, B. Lipphardt, S. Weyers, C. Tamm, and E. Peik, High-Accuracy Optical Clock Based on the Octupole Transition in $^{171}Yb^+$, Phys. Rev. Lett. **108**, 090801 (2012).

[27] M. Roberts, P. Taylor, S. V. Gateva-Kostova, R. B. M. Clarke, W. R. C. Rowley, and P. Gill, Measurement of the $^2S_{1/2}$-$^2D_{5/2}$ clock transition in a single $^{171}Yb^+$ ion, Phys. Rev. A **60**, 2867 (1999).

[28] C. H. Baldwin, B. J. Bjork, M. Foss-Feig, J. P. Gaebler, D. Hayes, M. G. Kokish, C. Langer, J. A. Sedlacek, D. Stack, and G. Vittorini, A high fidelity light-shift gate for clock-state qubits, Phys. Rev. A **103**, 012603 (2021).

[29] C. L. Edmunds, T. R. Tan, A. Milne, A. Singh, M. J. Biercuk, and C. Hempel, Scalable hyperfine qubit state detection via electron shelving in the $^2D_{5/2}$ and $^2F_{7/2}$ manifolds in $^{171}Yb^+$, Phys. Rev. A **104**, 012606 (2021).

[30] K. Sugiyama, Laser cooling of single $^{174}Yb^+$ ions stored in a RF trap, Jpn. J. Appl. Phys. **38**, 2141 (1999).

[31] Y.-Y. Jau, J. D. Hunker, and P. D. D. Schwindt, F-state quenching with CH_4 for buffer-gas cooled $^{171}Yb^+$ frequency standard, AIP Adv. **5**, 117209 (2015).

[32] S. Mulholland, H. A. Klein, G. P. Barwood, S. Donnellan, P. B. R. Nisbet-Jones, G. Huang, G. Walsh, P. E. G. Baird, and P. Gill, Compact laser system for a laser-cooled ytterbium ion microwave frequency standard, Rev. Sci. Instrum. **90**, 033105 (2019).

[33] C. L. Edmunds, C. Hempel, R. J. Harris, V. Frey, T. M. Stace, and M. J. Biercuk, Dynamically corrected gates suppressing spatiotemporal error correlations as measured by randomized benchmarking, Phys. Rev. Research **2**, 013156 (2020).

[34] A. D. Ludlow, M. M. Boyd, J. Ye, E. Peik, and P. O. Schmidt, Optical atomic clocks, Rev. Mod. Phys. **87**, 637 (2015).

[35] W. F. Meggers, The second spectrum of ytterbium (Yb II), J. Res. Nat. Bur. Stand. **71A**, 396 (1967).

[36] MOG Laboratories, Model CEL002.

[37] D. J. Thompson and R. E. Scholten, Narrow linewidth tunable external cavity diode laser using wide bandwidth filter, Rev. Sci. Instrum. **83**, 023107 (2012).

[38] R. W. Berends, E. H. Pinnington, B. Guo, and Q. Ji, Beam-laser lifetime measurements for four resonance levels of Yb II, J. Phys. B **26**, L701 (1993).

[39] S. A. Webster, P. E. Blythe, K. Hosaka, G. P. Barwood, and P. Gill, Systematics shifts of the 467 nm electric octupole transition in $^{171}Yb^+$, National Physical Laboratory Report No. CBTLM 31, 1999.

[40] P. Taylor, M. Roberts, G. M. Macfarlane, G. P. Barwood, W. R. C. Rowley, and P. Gill, Measurement of the infrared $^2F_{7/2}$−$^2D_{5/2}$ transition in a single $^{171}Yb^+$ ion, Phys. Rev. A **60**, 2829 (1999).

[41] P. Gill, H. A. Klein, A. P. Levick, M. Roberts, W. R. C. Rowley, and P. Taylor, Measurement of the $^2S_{1/2}$-$^2D_{5/2}$ 411-nm interval in laser-cooled trapped $^{171}Yb^+$ ions, Phys. Rev. A **52**, R909 (1995).

[42] H. A. Fürst, C.-H. Yeh, D. Kalincev, A. P. Kulosa, L. S. Dreissen, R. Lange, E. Benkler, N. Huntemann, E. Peik, and T. E. Mehlstäubler, Coherent Excitation of the Highly Forbidden Electric Octupole Transition in $^{172}Yb^+$, Phys. Rev. Lett. **125**, 163001 (2020).

[43] W. C. Martin and W. L. Wiese, *Atomic, Molecular, and Optical Physics Handbook*, edited by G. W. F. Drake, National Institute of Standards and Technology (AIP Press, Woodbury, NY, 1996), Chap. 10; http://physics.nist.gov/Pubs/AtSpec/index.html.

[44] Wayne M. Itano, External-field shifts of the $^{199}Hg^+$ optical frequency standard, J. Res. Nat. Inst. Standards Technol. **105**, 829 (2000).

[45] J. Vanier and C. Audoin, *The Quantum Physics of Atomic Frequency Standards* (A. Hilger Publishers, Philadelphia, 1989).

[46] N. J. Stone, Nuclear magnetic dipole and electric quadrupole moments: Their measurement and tabulation as accessible data, J. Phys. Chem. Ref. Data **44**, 031215 (2015).

[47] H. C. J. Gan, G. Maslennikov, K.-W. Tseng, T. R. Tan, R. Kaewuam, K. J. Arnold, D. Matsukevich, and M. D. Barrett, Oscillating-magnetic-field effects in high-precision metrology, Phys. Rev. A **98**, 032514 (2018).